

Pinwheel valence bond crystal ground state of the spin- $\frac{1}{2}$ Heisenberg antiferromagnet on the shuriken lattice

Nikita Astrakhantsev,^{1,2,*} Francesco Ferrari^{3,*} Nils Niggemann^{4,*} Tobias Müller,⁵ Aishwarya Chauhan^{6,6} Augustine Kshetrimayum^{4,7} Pratyay Ghosh,⁵ Nicolas Regnault⁸ Ronny Thomale,^{5,6} Johannes Reuther,^{4,7} Titus Neupert^{4,1} and Yasir Iqbal^{6,†}

¹Department of Physics, University of Zürich, Winterthurerstrasse 190, CH-8057 Zürich, Switzerland

²Institute for Theoretical and Experimental Physics (ITEP), Moscow 117218, Russia

³Institut für Theoretische Physik, Goethe-Universität Frankfurt, Max-von-Laue-Straße 1, D-60438 Frankfurt am Main, Germany

⁴Dahlem Center for Complex Quantum Systems and Institut für Theoretische Physik, Freie Universität Berlin, Arnimallee 14, D-14195 Berlin, Germany

⁵Institut für Theoretische Physik und Astrophysik, Julius-Maximilians-Universität Würzburg, Am Hubland, D-97074 Würzburg, Germany

⁶Department of Physics and Quantum Centers in Diamond and Emerging Materials (QuCenDiEM) group, Indian Institute of Technology Madras, Chennai 600036, India

⁷Helmholtz-Zentrum Berlin für Materialien und Energie, Hahn-Meitner-Platz 1, D-14109 Berlin, Germany

⁸Joseph Henry Laboratories and Department of Physics, Princeton University, Princeton, New Jersey 08544, USA



(Received 20 October 2021; accepted 3 December 2021; published 22 December 2021)

We investigate the nature of the ground state of the spin- $\frac{1}{2}$ Heisenberg antiferromagnet on the shuriken lattice by complementary state-of-the-art numerical techniques, such as variational Monte Carlo (VMC) with versatile Gutzwiller-projected Jastrow wave functions, unconstrained multivariable variational Monte Carlo (mVMC), and pseudofermion/pseudo-Majorana functional renormalization group (PFFRG/PMFRG) methods. We establish the presence of a quantum paramagnetic ground state and investigate its nature, by classifying symmetric and chiral quantum spin liquids, and inspecting their instabilities towards competing valence bond crystal (VBC) orders. Our VMC analysis reveals that a VBC with a pinwheel structure emerges as the lowest-energy variational ground state, and it is obtained as an instability of the U(1) Dirac spin liquid. Analogous conclusions are drawn from mVMC calculations employing accurate BCS pairing states supplemented by symmetry projectors, which confirm the presence of pinwheel VBC order by a thorough analysis of dimer-dimer correlation functions. Our work highlights the nontrivial role of quantum fluctuations via the Gutzwiller projector in resolving the subtle interplay between competing orders.

DOI: [10.1103/PhysRevB.104.L220408](https://doi.org/10.1103/PhysRevB.104.L220408)

Introduction. The kagome lattice, which has played such a decisive role in the higher echelons of frustrated magnetism, owes much of its intriguing physics to the corner-sharing arrangement of triangular motifs. This geometry leads to only a *marginal* alleviation of frustration in a system of antiferromagnetically interacting spins, and in essence accounts for the appearance of novel quantum paramagnetic phases such as quantum spin liquids. In this Letter, we consider the much less explored non-Archimedean [1] variant of the two-dimensional corner-sharing arrangement of triangles, namely the shuriken lattice [2] (also referred to as the square-kagome or squagome lattice in literature) (see Fig. 1). Following the recent experimental reporting of a gapless spin liquid in a first material realization of the shuriken geometry by spin $S = 1/2$ Cu^{2+} magnetic ions in $\text{KCu}_6\text{AlBiO}_4(\text{SO}_4)_5\text{Cl}$ [3], there is renewed interest in exploring the nature of frustration-induced phases in the quantum Heisenberg antiferromagnet.

In this Letter, we investigate the ground state of the Heisenberg antiferromagnetic model

$$\hat{\mathcal{H}} = J \sum_{\langle i,j \rangle} \hat{\mathbf{S}}_i \cdot \hat{\mathbf{S}}_j \quad (1)$$

for $S = 1/2$ operators $\hat{\mathbf{S}}_i = (\hat{S}_i^x, \hat{S}_i^y, \hat{S}_i^z)$ decorated on the shuriken lattice, where the two symmetry inequivalent exchange couplings, i.e., on the square (J_{\square}) and triangular (J_{Δ}) bonds [see Fig. 1(a)] are taken as equal and denoted by $J (= J_{\Delta} = J_{\square})$ [see Fig. 1(a) and Supplemental Material (SM) [7]]. We employ (i) variational Monte Carlo (VMC) with Gutzwiller-projected fermionic wave functions on large system sizes (up to 2400 sites), (ii) many-variable variational Monte Carlo (mVMC) involving an unconstrained optimization of a BCS pairing function on system sizes up to 384 sites, and (iii) a pseudofermion functional renormalization group (PFFRG) analysis to firmly establish the absence of long-range magnetic order in the ground state of (1), which remained to be conclusively shown within exact diagonalization [4,5,8–10], mean-field [11], and perturbative [12,13] schemes. To identify the precise nature of the quantum

*These authors contributed equally to this work.

†yiqbal@physics.iitm.ac.in

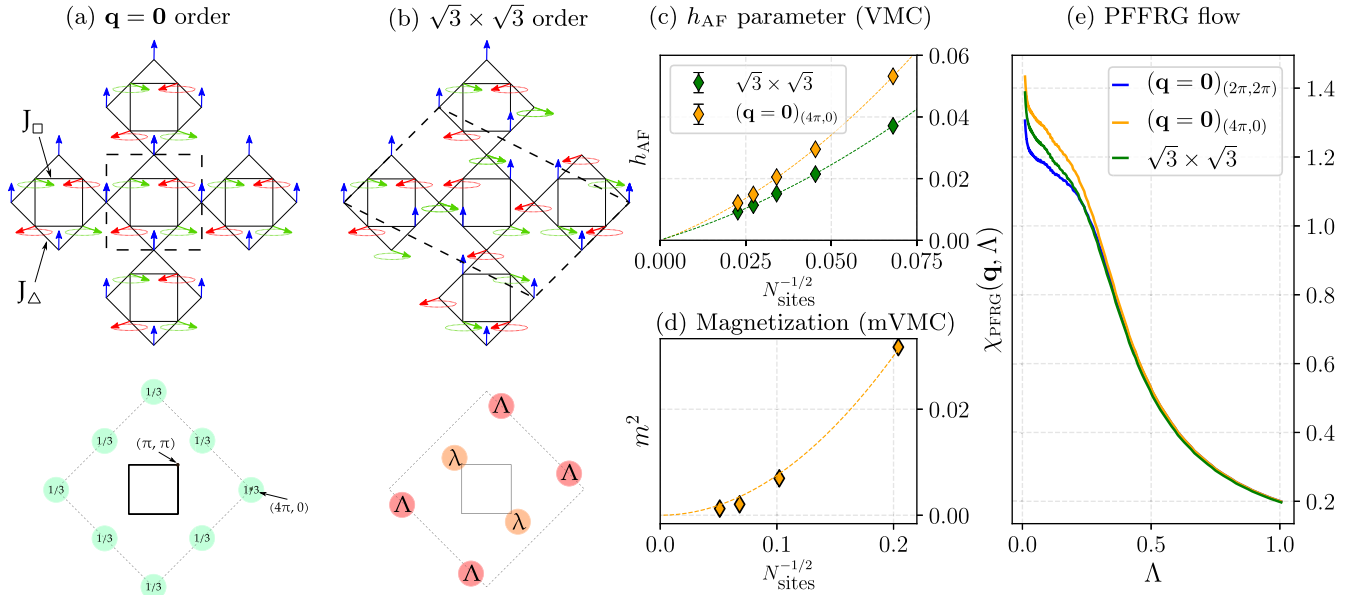


FIG. 1. (a), (b) Top row: Illustration of two types of magnetic orders within the ground-state manifold of the classical Heisenberg antiferromagnet on the shuriken lattice [4,5]. The two symmetry inequivalent nearest-neighbor bonds are labeled as J_Δ and J_\square . The $\mathbf{q} = \mathbf{0}$ ($\sqrt{3} \times \sqrt{3}$) order has an angle of 120° between neighboring spins, and a magnetic unit cell which is identical (three times enlarged) compared to the six-site geometrical unit cell is marked by a dashed line. The green ellipses depict further degrees of freedom present in the classically degenerate ground-state manifold. Bottom row: The first (solid line) and extended (dashed line) Brillouin zones of the shuriken lattice showing the location of the Bragg peaks with the fraction of the total spectral weight of the classical (a) $\mathbf{q} = \mathbf{0}$ order, at $(4\pi, 0)$ and $(2\pi, 2\pi)$ (and symmetry related points) with equal spectral weight, and (b) $\sqrt{3} \times \sqrt{3}$ order, at $(2\pi \pm q, 2\pi \mp q)$ with $q = 4\pi/3$, and leading subdominant peaks at $(q, -q)$ with 36%, i.e., $\lambda/\Lambda = 0.36$, of the spectral weight of the dominant ones [6]. The $\sqrt{3} \times \sqrt{3}$ order breaks the fourfold rotational symmetry. From (c) VMC, the size scaling of the h_{AF} parameter (fictitious Zeeman field [7]) for $\mathbf{q} = \mathbf{0}$ and $\sqrt{3} \times \sqrt{3}$ orders on finite clusters of $N_{\text{sites}} = 6L^2$ sites, with $L = 6, 9, 12, 15$, and 18 (quadratic fit), (d) mVMC, the size scaling of the sublattice magnetization for the $\mathbf{q} = \mathbf{0}$ order finite clusters of $N_{\text{sites}} = 6L^2$ sites, with $L = 2, 4, 6$, and 8 (quadratic fit), and (e) PFFRG, the RG flow of the susceptibility tracked at the dominant ordering vectors of the two classical orders.

paramagnetic ground state, we construct symmetric and chiral U(1) fermionic mean-field *Ansätze* of quantum spin liquids, compute their projected energies, and investigate their potential instability towards competing VBC orders which have been proposed within a quantum dimer model approach [5,13] and a large- N analysis [2]. Our study finds an instability of the U(1) Dirac spin liquid towards a pinwheel (PW) VBC order with a 2×2 expanded, i.e., 24-site unit cell [5,13], which emerges as the lowest-energy variational state, in contrast to the findings in Ref. [13] which claimed for the stabilization of a loop-6 (L6) VBC (see also Fig. 2). An unconstrained mVMC optimization of the BCS pairing function starting from a random choice of pairing amplitudes is also found to converge to a long-range dimer-ordered ground state with a PW-VBC type structure, as revealed from the dimer-dimer correlation functions. These findings are further corroborated by a PFFRG analysis of the dimer-response functions. The estimates of the ground-state energy on finite clusters obtained within VMC by the application of a couple of Lanczos steps to the PW-VBC state supplemented by a zero-variance extrapolation, as well as those obtained from mVMC are found to be in excellent agreement. The respective estimates in the thermodynamic limit obtained by finite-size scaling are in good agreement with those obtained from our infinite projected entangled pair state (iPEPS) and pseudo-Majorana functional renormalization group (PMFRG) calculations, thus lending strong evidence in favor of a PW-VBC ground state

of the $S = 1/2$ Heisenberg antiferromagnet on the shuriken lattice.

Results. We start by employing fermionic VMC [14] to investigate the possible presence of magnetically ordered ground states with two different periodicities: (i) a translationally invariant, i.e., $\mathbf{q} = \mathbf{0}$ state [see Fig. 1(a)] and (ii) the so-called $\sqrt{3} \times \sqrt{3}$ state [see Fig. 1(b)]. Details on the form of the variational wave functions are given in the Supplemental Material (SM) [7] (see also Refs. [15–31]). The Zeeman field variational parameter h_{AF} extrapolates to zero in the thermodynamic limit [see Fig. 1(c)], indicating the absence of long-range magnetic order in the ground state. Additional evidence is provided by mVMC calculations (see SM [7] and also Refs. [32–39]), in which the sublattice magnetization m^2 is computed by evaluating the spin-spin correlation $\langle \hat{\mathbf{S}}_i \cdot \hat{\mathbf{S}}_j \rangle$ at maximum distance (for two spins i, j within the same sublattice) [40], where $\langle \dots \rangle$ denotes the expectation value over the variational state $|\phi_{\text{pair}}\rangle$ [7]. The sublattice magnetization is seen to display a similar size scaling as the h_{AF} parameter of VMC [see Fig. 1(d)], thus confirming the absence of magnetic order. These results are further corroborated by a PFFRG analysis (see SM [7] and Refs. [41–62]) which does not find in the RG flow any evidence for a divergence or a breakdown of the susceptibility at the ordering wave vectors of either the $\mathbf{q} = \mathbf{0}$ or $\sqrt{3} \times \sqrt{3}$ orders [see Fig. 1(e)].

Thus, having established the paramagnetic character of the ground state, we proceed towards deciphering its

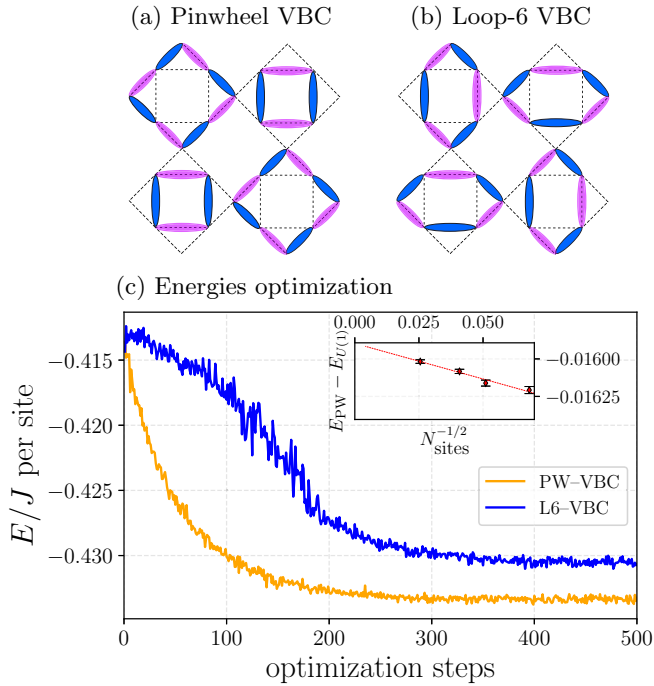


FIG. 2. Two competing dimer orders, (a) PW-VBC and (b) L6-VBC on the shuriken lattice. Both dimer states are eightfold degenerate. (c) The evolution of the energy per site during a typical VMC optimization for the VBCs, here shown for Hamiltonian (1) on the $L = 20$ cluster. The inset shows the finite-size scaling of the energy gain of the PW-VBC state with respect to the U(1) DSL.

nature. To this end, we construct a family of fully symmetric and chiral fermionic mean-field *Ansätze* with a U(1) gauge structure based on a symmetry classification of flux patterns. These *Ansätze* are completely determined by specifying the fluxes threading three distinct plaquettes within the unit cell of the lattice: vertically oriented triangles (Φ_{Δ}), horizontally oriented triangles (Φ_{\triangleright}), and squares (Φ_{\square}). Henceforth, we label the mean-field *Ansätze* by specifying the flux triad ($\Phi_{\Delta}, \Phi_{\triangleright}, \Phi_{\square}$). We obtain four distinct fully symmetric U(1) spin liquids (see Table I and SM [7]), and several chiral states out of which we focus only on those with a $\pi/2$ flux through triangles. In Table I, we present the energies of the (self-consistent) mean-field and Gutzwiller-projected wave functions for these states. At the mean-field level, the chiral $(\frac{\pi}{2}, \frac{\pi}{2}, \pi)$ state has the lowest energy, in complete compliance with the Rokhsar rules [63,64]. However, after Gutzwiller projection, the chiral spin liquid is no longer energetically competitive, and the $(0,0,0)$ flux uniform *Ansatz* featuring a spinon Fermi surface (SFS) emerges as the lowest-energy spin-liquid state, followed by the $(0, 0, \pi)$ state which is a U(1) Dirac spin liquid (DSL). Since, in two spatial dimensions, the U(1) SFS and DSL are potentially susceptible to gap opening instabilities [65,66], we investigate their potential instability towards previously proposed VBC candidates [5,13].

A quantum dimer model treatment of (1), truncated to a minimal nearest-neighbor valence bond basis, identified a PW-VBC with C_4 symmetry and loop-4 resonances [5] [see Fig. 2(a)]. This picture was subsequently challenged in

TABLE I. For Hamiltonian (1), we present the mean-field (MF) and Gutzwiller-projected (proj.) ground-state energy per site (in units of J) on the $4 \times 4 \times 6$ cluster for the different fully symmetric (FS) and chiral U(1) quantum spin liquid *Ansätze* (see Fig. S4 of SM [7]) labeled by the flux triad ($\Phi_{\Delta}, \Phi_{\triangleright}, \Phi_{\square}$) (see text), as well as dimer states. The $(\pi, 0, 0)$ and $(\pi, 0, \pi)$ *Ansätze* have extensively degenerate levels at half filling which prevents a computation of their energy (as the wave function cannot be uniquely defined).

Ansatz	Fluxes	MF energy	Proj. energy	MF spectrum
FS	(0,0,0)	-0.36570	-0.42714(2)	Fermi surface
	(0, 0, π)	-0.38388	-0.41720(3)	Dirac points
	$(\pi, 0, 0)$	-0.36657		Flat band
	$(\pi, 0, \pi)$	-0.37130	-0.41362(3)	Fermi surface
Chiral	$(\frac{\pi}{2}, \frac{\pi}{2}, 0)$	-0.35041		Flat band
	$(\frac{\pi}{2}, \frac{\pi}{2}, \pi)$	-0.39803	-0.40489(3)	Gapped
	$(\frac{\pi}{2}, -\frac{\pi}{2}, 0)$	-0.38040	-0.38702(4)	Fermi surface
	$(\frac{\pi}{2}, -\frac{\pi}{2}, \pi)$	-0.36123	-0.40205(3)	Fermi surface
Dimer	L6-VBC	-0.41013	-0.43009(1)	Gapped
	PW-VBC	-0.40623	-0.43333(1)	Gapped

Ref. [13] by a L6-VBC with loop-6 resonances [see Fig. 2(b)] when accounting for a basis beyond nearest-neighbors. In particular, it was argued that the virtually excited long-range singlets that are induced around defect triangles lead to an enhancement of loop-6 resonances compared to loop-4, helping stabilize the L6-VBC *in lieu* of the PW-VBC [13]. Here, we investigate the energetic competition between PW-VBC and L6-VBC orders within VMC and mVMC wherein the effect of quantum fluctuations is captured via the Gutzwiller projector. To construct variational VBC states within VMC, we consider each of the symmetric spin-liquid *Ansätze* listed in Table I, and allow the hopping amplitudes to take different values according to the dimer pattern of the strong/weak symmetry inequivalent bonds within the 24-site VBC unit cells [67]. Our study reveals that while the SFS spin liquid remains robust to both these VBC perturbations, the U(1) Dirac spin liquid destabilizes towards both these VBCs, with the PW-VBC yielding a lower energy [see Fig. 2(c) and Table I]. It is interesting to note that at the self-consistent mean-field level the L6-VBC has a lower energy compared to the PW-VBC, but the relative hierarchy is inverted in favor of the PW-VBC once the Gutzwiller projector is enforced within VMC, highlighting the role of quantum fluctuations in resolving the delicate competition of these two dimerized states. Furthermore, VMC calculations show that the energy gain of the PW-VBC relative to the U(1) Dirac spin liquid remains finite in the thermodynamic limit [see the inset of Fig. 2(c)] indicating the size consistency of the PW-VBC state, thereby lending support to it being a stable variational ground state in the thermodynamic limit. The energy of the PW-VBC *Ansatz* is found to be lower compared to the SFS spin-liquid state, thus representing the optimal wave function within our VMC calculations.

To obtain competitive wave functions within mVMC, we impose a 2×2 unit cell periodicity on the parameters of the variational state $|\phi_{\text{pair}}\rangle$. The properties of the optimized wave function are assessed by measuring the dimer-dimer correlation function $\chi_{b,b'}^D = \langle \hat{D}_b \hat{D}_{b'} \rangle - \langle \hat{D}_b \rangle \langle \hat{D}_{b'} \rangle$ for all pairs of

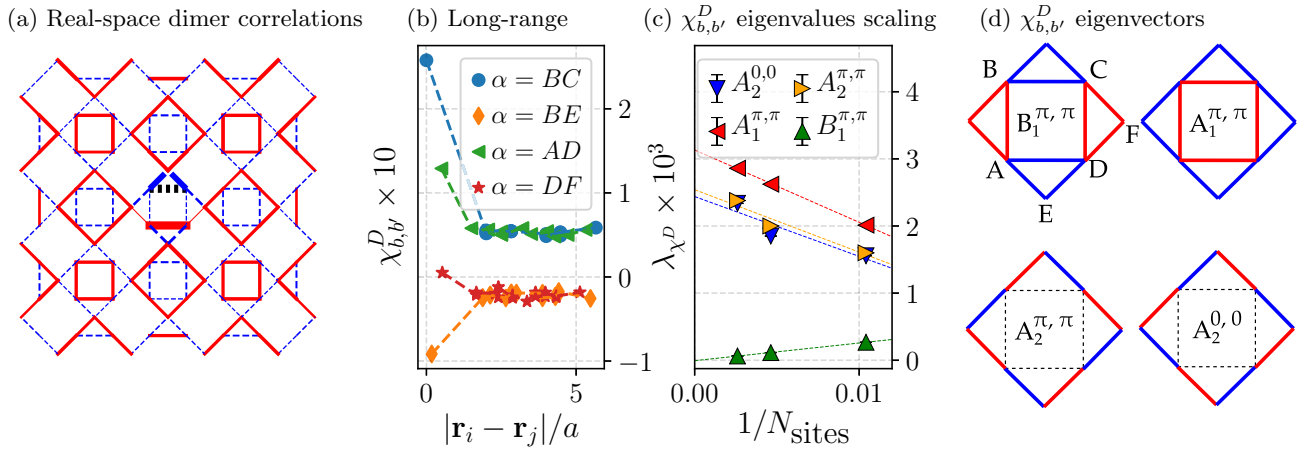


FIG. 3. (a) Dimer-dimer correlations between the base bond (between sublattice B and C sites [7]), marked by a black dotted line, and other bonds measured within mVMC on the $L = 8$ cluster. Solid red (dashed blue) lines represent positive (negative) correlation values. An analogous figure with the base bond on the side of a triangle can be found in SM [7]. (b) Long-range correlations between the base bond and other bonds labeled by α . Only correlations between the $(0,0)$ and $(2n, 2m)$ unit cells are shown due to the alternating 2×2 pattern in bond correlations. (c) Infinite-volume extrapolation of the largest eigenvalues of χ^D . (d) The dominant eigenvectors of χ^D : Red bonds are positive, while blue are negative and other bonds are zero. In the middle of each drawing, the high-symmetry momentum of the representation is shown, as well as the corresponding irreducible representation label of the D_4 point symmetry group.

bonds in the system, $0 \leq b, b' < N_{\text{bonds}}$, where $\hat{D}_b = \hat{\mathbf{S}}_i \cdot \hat{\mathbf{S}}_j$, with i, j being sites at ends of the bond b . In Fig. 3(a), we show the dimer-dimer correlations between the base (square) bond and other bonds lying within few unit cells, which display the characteristic pinwheel structure found also within VMC. To carry out a quantitative assessment of the VBC character of the ground state, we need to define suitable scalar order parameters to perform an infinite-volume extrapolation of the dimer order. Thus, we regard $\chi_{b,b'}^D$ as a matrix in the bond indices and we diagonalize it; the resulting set of eigenvalues/eigenvectors pairs (λ, A_b^λ) is used to define the operators $\hat{O}_\lambda = \sum_b A_b^\lambda \hat{D}_b$, each of them corresponding to a certain momentum and irreducible representation of the lattice point group. The tendency to establish a finite expectation value of one of these operators, and thus spontaneously break the corresponding lattice symmetry, is measured by the susceptibility $\chi_{\hat{O}_\lambda} = \langle \hat{O}_\lambda^\dagger \hat{O}_\lambda \rangle - \langle \hat{O}_\lambda^\dagger \rangle \langle \hat{O}_\lambda \rangle = \lambda$ extrapolated to thermodynamic limit [68].

This extrapolation requires a knowledge of the order parameter scaling law. We argue that $1/L^2$, i.e., inverse-volume scaling, is a suitable choice. To check that, in Fig. 3(b) we show long-range behavior of correlations between the base bond [BC in the $(0,0)$ unit cell] and bonds in the other unit cells with the bond within the unit cell labeled by α [see Fig. 3(d)]. We observe that (i) the correlator saturates almost immediately with distance, suggesting exponential decay finite-range corrections to correlations, and (ii) correlations between the base bond and bonds with different α converge to *different and finite* values, which paves the way to finite susceptibility $\chi_{\hat{O}_\lambda}$ for some symmetry-breaking operator \hat{O}_λ .

In Fig. 3(d), we depict the leading eigenvectors of $\chi_{b,b'}^D$, and in Fig. 3(c) show the infinite-volume extrapolation of the corresponding eigenvalues λ (i.e., of the susceptibilities $\chi_{\hat{O}_\lambda}$). We observe that the susceptibilities corresponding to the

$A_1^{\pi,\pi}$ and $A_2^{\pi,\pi}$ irreducible representations, which are reflective of the PW-VBC phase symmetry structure, clearly extrapolate to finite values, while the $B_1^{\pi,\pi}$ irreducible representation susceptibility indicating a L6-VBC phase structure is found to vanish (within error bars) in the thermodynamic limit.

We also probe, within PFFRG, the tendency towards PW-VBC and L6-VBC symmetry-breaking patterns, and observe that although the dimer-response functions for these two orders get enhanced under RG flow indicating dimerization, they are of similar magnitude [7]. The absence of a categorical identification of the dimerization tendency within PFFRG is rooted in the fact that one does not take into account higher-point vertex functions which ultimately seem to prove decisive in accurately resolving the delicate competition between the two VBC candidates.

Having established, from both VMC and mVMC, that the ground state of the system possesses long-range dimer order, we discuss other static quantities, namely the extrapolation of the ground-state energy, reported in Fig. 4, and the equal-time spin structure factor, shown in Fig. 5. Within VMC, an improved estimate of the ground-state energy on finite clusters can be achieved by applying a few Lanczos steps to the variational state (here the PW-VBC), and performing a zero-variance extrapolation [15,27–31]. The resulting estimate of the ground-state energy is found to be equal (within three error bars) with the mVMC energies on the $L = 4, 6,$ and 8 clusters. Furthermore, the finite-size scaling estimates of the thermodynamic ground-state energy from VMC and mVMC,

$$E_{\text{mVMC}}^\infty = -0.43696(17), \quad E_{\text{VMC}}^\infty = -0.43730(13) \quad (2)$$

are equal within two error bars and in excellent agreement with that obtained from iPEPS (see SM [7] and Refs. [69–81]) and consistent with PMFRG (see SM [7] and Refs. [82–85]) at finite temperature directly in the thermodynamic limit. Finally, the (equal-time) static spin structure factor $S(\mathbf{q})$ [7]

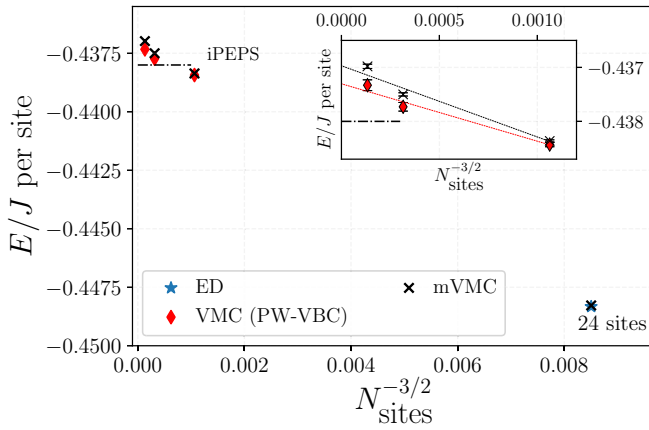


FIG. 4. The ground-state energies on the $L = 4, 6,$ and 8 clusters obtained from VMC and mVMC together with the inset showing the finite-size scaling. The blue star denotes the exact diagonalization (ED) energy on the D_4 symmetric 6×2^2 cluster, and the iPEPS energy (obtained by a quadratic fit for the three largest bond dimensions) is marked by a horizontal dashed line [7].

for the PW-VBC ground state obtained from both VMC and mVMC approaches is shown in Fig. 5. One observes a diffused distribution of intensity along the extended Brillouin zone boundaries. We observe that within VMC the estimate of the ground state $S(\mathbf{q})$ obtained by applying two Lanczos steps on the bare PW-VBC wave function displays soft maxima in close vicinity to the pinch points [Fig. 5(a)] seen in a large- N analysis (Fig. S2 of SM [7]) in conformity with mVMC [Fig. 5(b)].

Conclusions. We have employed state-of-the-art numerical quantum many-body methods to provide compelling evidence that the ground state of the $S = 1/2$ Heisenberg antiferromagnet on the shuriken lattice features long-range dimer-order breaking translational invariance, i.e., a VBC. Combining the two variational methods, (i) VMC with *a priori* given different QSL and VBC *Ansätze*, and (ii) mVMC involving an unconstrained optimization of the projected-BCS wave function, we have revealed a consistent picture of a VBC with a pinwheel structure of correlations as inferred from a comprehensive analysis of the dimer-dimer correlation function. This finding is at variance with that obtained within an extended

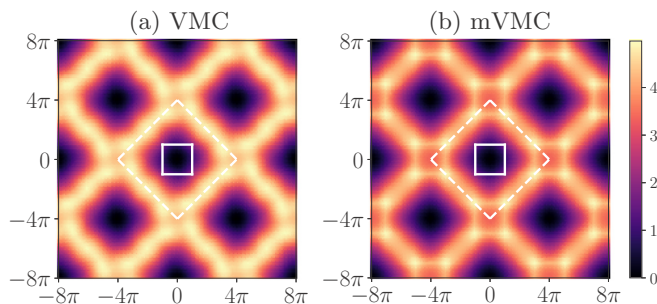


FIG. 5. The static (equal-time) spin structure factor $S(\mathbf{q})$ obtained within (a) VMC and (b) mVMC on the $L = 8$ cluster. The solid (dashed) white lines mark the first (extended) Brillouin zones.

(beyond nearest-neighbor valence bond basis) quantum dimer model framework which argued for a loop-6 VBC [13]. Given that $\text{KCu}_6\text{AlBiO}_4(\text{SO}_4)_5\text{Cl}$ [3] realizes a gapless spin liquid, and consideration of a generalized model with $J_\Delta \neq J_\square$ and further neighbor couplings fails to reproduce the neutron scattering profile as shown in Ref. [3], possibly hints at the role of non-negligible Dzyaloshinskii-Moriya interactions at play, and the investigation of these interactions would constitute an important future direction of research. Finally, given that (lattice) nematic topological quantum spin liquids have been proposed as competitive *Ansätze* [11], a projective symmetry group classification [18] of fermionic mean-field *Ansätze* of symmetric and nematic \mathbb{Z}_2 spin liquids, and a subsequent analysis of the energies and correlation functions of the corresponding Gutzwiller-projected spin states would constitute an important direction for future investigations.

Acknowledgments. We thank Arnaud Ralko, Ludovic Jaubert, Atanu Maity, and Federico Becca for illuminating discussions. Y.I. acknowledges financial support by the Science and Engineering Research Board (SERB), Department of Science and Technology (DST), India through the Startup Research Grant No. SRG/2019/000056, MATRICS Grant No. MTR/2019/001042, and the Indo-French Centre for the Promotion of Advanced Research (CEFIPRA) Project No. 64T3-1. This research was supported in part by the National Science Foundation under Grant No. NSF PHY-1748958, the Abdus Salam International Centre for Theoretical Physics (ICTP) through the Simons Associateship scheme funded by the Simons Foundation, IIT Madras through the Institute of Eminence (IoE) program for establishing the QuCenDiEM group (Project No. SB20210813PHMHRD002720) and FORG group (Project No. SB20210822PHMHRD008268), the International Centre for Theoretical Sciences (ICTS), Bengaluru, India during a visit for participating in the program “Novel phases of quantum matter” (Code: ICTS/topmatter2019/12). Y.I. acknowledges the use of the computing resources at HPCE, IIT Madras. F.F. acknowledges support from the Alexander von Humboldt Foundation through a postdoctoral Humboldt fellowship. N.A. is funded by the Swiss National Science Foundation, Grant No. PP00P2_176877. The mVMC simulations (Results section) were supported by the Russian Science Foundation (RSF) grant (Project No. 21-12-00237). The authors acknowledge the usage of computing resources of the federal collective usage center “Complex for simulation and data processing for mega-science facilities” at NRC “Kurchatov Institute” [86]. N.N. acknowledges funding from the German Research Foundation within the TRR 183 (project A04) and the usage of computing resources at the Curta cluster provided by the ZEDAT [87]. The work in Würzburg was supported by the Deutsche Forschungsgemeinschaft (DFG, German Research Foundation) through Project-ID 258499086-SFB 1170 and the Würzburg-Dresden Cluster of Excellence on Complexity and Topology in Quantum Matter - ct.qmat Project-ID 390858490-EXC 2147. T.M., P.G., and R.T. gratefully acknowledge the Gauss Centre for Supercomputing e.V. [88] for funding this project by providing computing time on the GCS Supercomputer SuperMUC at Leibniz Supercomputing Centre [89].

- [1] A non-Archimedean lattice has two or more sets of topologically distinct sites. For the shuriken lattice it is two, those sites which are the vertices of squares and those which are not.
- [2] R. Siddharthan and A. Georges, Square kagome quantum antiferromagnet and the eight-vertex model, *Phys. Rev. B* **65**, 014417 (2001).
- [3] M. Fujihala, K. Morita, R. Mole, S. Mitsuda, T. Tohyama, S.-i. Yano, D. Yu, S. Sota, T. Kuwai, A. Koda, H. Okabe, H. Lee, S. Itoh, T. Hawai, T. Masuda, H. Sagayama, A. Matsuo, K. Kindo, S. Ohira-Kawamura, and K. Nakajima, Gapless spin liquid in a square-kagome lattice antiferromagnet, *Nat. Commun.* **11**, 3429 (2020).
- [4] J. Richter, J. Schulenburg, P. Tomczak, and D. Schmalfuß, The Heisenberg antiferromagnet on the square-kagomé lattice, *Condens. Matter Phys.* **12**, 507 (2009).
- [5] I. Rousochatzakis, R. Moessner, and J. van den Brink, Frustrated magnetism and resonating valence bond physics in two-dimensional kagome-like magnets, *Phys. Rev. B* **88**, 195109 (2013).
- [6] Additional subdominant Bragg peaks, carrying (i) 12% of the spectral weight of the dominant ones are located at $(2\pi - q, q)$, $(q, 2\pi - q)$, $[-(2\pi - q), 2q]$, and $[2q, -(2\pi - q)]$ and (ii) carrying 4% intensity at $[-(2\pi - q), 2\pi - q]$, $(q, 2q)$, and $(2q, q)$.
- [7] See Supplemental Material at <http://link.aps.org/supplemental/10.1103/PhysRevB.104.L220408> for details on the methodological details for VMC, mVMC, PFFRG, PMFRG, large- N , and Luttinger-Tisza approaches employed.
- [8] H. Nakano and T. Sakai, The two-dimensional $S = 1/2$ Heisenberg antiferromagnet on the shuriken lattice - A lattice composed of vertex-sharing triangles, *J. Phys. Soc. Jpn.* **82**, 083709 (2013).
- [9] K. Morita and T. Tohyama, Magnetic phase diagrams and magnetization plateaus of the spin-1/2 antiferromagnetic Heisenberg model on a square-kagome lattice with three nonequivalent exchange interactions, *J. Phys. Soc. Jpn.* **87**, 043704 (2018).
- [10] Y. Hasegawa, H. Nakano, and T. Sakai, Metamagnetic jump in the spin- $\frac{1}{2}$ antiferromagnetic Heisenberg model on the square kagome lattice, *Phys. Rev. B* **98**, 014404 (2018).
- [11] T. Lugan, L. D. C. Jaubert, and A. Ralko, Topological nematic spin liquid on the square kagome lattice, *Phys. Rev. Research* **1**, 033147 (2019).
- [12] P. Tomczak and J. Richter, Specific heat of the spin- Heisenberg antiferromagnet on squagome lattice, *J. Phys. A* **36**, 5399 (2003).
- [13] A. Ralko and I. Rousochatzakis, Resonating-Valence-Bond Physics Is Not Always Governed by the Shortest Tunneling Loops, *Phys. Rev. Lett.* **115**, 167202 (2015).
- [14] F. Becca and S. Sorella, *Quantum Monte Carlo Approaches for Correlated Systems* (Cambridge University Press, Cambridge, UK, 2017).
- [15] Y. Iqbal, W.-J. Hu, R. Thomale, D. Poilblanc, and F. Becca, Spin liquid nature in the Heisenberg J_1 - J_2 triangular antiferromagnet, *Phys. Rev. B* **93**, 144411 (2016).
- [16] F. Ferrari, S. Bieri, and F. Becca, Competition between spin liquids and valence-bond order in the frustrated spin- $\frac{1}{2}$ Heisenberg model on the honeycomb lattice, *Phys. Rev. B* **96**, 104401 (2017).
- [17] Y. Iqbal, F. Ferrari, A. Chauhan, A. Parola, D. Poilblanc, and F. Becca, Gutzwiller projected states for the J_1 - J_2 Heisenberg model on the kagome lattice: Achievements and pitfalls, *Phys. Rev. B* **104**, 144406 (2021).
- [18] X.-G. Wen, Quantum orders and symmetric spin liquids, *Phys. Rev. B* **65**, 165113 (2002).
- [19] S. Bieri, C. Lhuillier, and L. Messio, Projective symmetry group classification of chiral spin liquids, *Phys. Rev. B* **93**, 094437 (2016).
- [20] Y. Iqbal, F. Becca, and D. Poilblanc, Valence-bond crystals in the kagomé spin-1/2 Heisenberg antiferromagnet: A symmetry classification and projected wave function study, *New J. Phys.* **14**, 115031 (2012).
- [21] Y. Iqbal, F. Becca, and D. Poilblanc, Projected wave function study of \mathbb{Z}_2 spin liquids on the kagome lattice for the spin- $\frac{1}{2}$ quantum Heisenberg antiferromagnet, *Phys. Rev. B* **84**, 020407 (2011).
- [22] Y. Iqbal, D. Poilblanc, and F. Becca, Spin- $\frac{1}{2}$ Heisenberg J_1 - J_2 antiferromagnet on the kagome lattice, *Phys. Rev. B* **91**, 020402 (2015).
- [23] Y. Iqbal, F. Becca, and D. Poilblanc, Valence-bond crystal in the extended kagome spin- $\frac{1}{2}$ quantum Heisenberg antiferromagnet: A variational Monte Carlo approach, *Phys. Rev. B* **83**, 100404 (2011).
- [24] S. Sorella, Green Function Monte Carlo with Stochastic Reconfiguration, *Phys. Rev. Lett.* **80**, 4558 (1998).
- [25] S. Yunoki and S. Sorella, Two spin liquid phases in the spatially anisotropic triangular Heisenberg model, *Phys. Rev. B* **74**, 014408 (2006).
- [26] N. Laflorencie and D. Poilblanc, Simulations of pure and doped low-dimensional spin-1/2 gapped systems, *Lect. Notes Phys.* **645**, 227 (2004).
- [27] S. Sorella, Generalized Lanczos algorithm for variational quantum Monte Carlo, *Phys. Rev. B* **64**, 024512 (2001).
- [28] F. Becca, W.-J. Hu, Y. Iqbal, A. Parola, D. Poilblanc, and S. Sorella, Lanczos steps to improve variational wave functions, *J. Phys.: Conf. Ser.* **640**, 012039 (2015).
- [29] Y. Iqbal, F. Becca, S. Sorella, and D. Poilblanc, Gapless spin-liquid phase in the kagome spin- $\frac{1}{2}$ Heisenberg antiferromagnet, *Phys. Rev. B* **87**, 060405(R) (2013).
- [30] Y. Iqbal, D. Poilblanc, and F. Becca, Vanishing spin gap in a competing spin-liquid phase in the kagome Heisenberg antiferromagnet, *Phys. Rev. B* **89**, 020407(R) (2014).
- [31] Y. Iqbal, D. Poilblanc, R. Thomale, and F. Becca, Persistence of the gapless spin liquid in the breathing kagome Heisenberg antiferromagnet, *Phys. Rev. B* **97**, 115127 (2018).
- [32] T. Misawa, S. Morita, K. Yoshimi, M. Kawamura, Y. Motoyama, K. Ido, T. Ohgoe, M. Imada, and T. Kato, mVMC-Open-source software for many-variable variational Monte Carlo method, *Comput. Phys. Commun.* **235**, 447 (2019).
- [33] T. Misawa, Y. Nomura, S. Biermann, and M. Imada, Self-optimized superconductivity attainable by interlayer phase separation at cuprate interfaces, *Sci. Adv.* **2**, e1600664 (2016).
- [34] T. Misawa and M. Imada, Origin of high- T_c superconductivity in doped Hubbard models and their extensions: Roles of uniform charge fluctuations, *Phys. Rev. B* **90**, 115137 (2014).
- [35] M. Casula, C. Attaccalite, and S. Sorella, Correlated geminal wave function for molecules: An efficient resonating valence bond approach, *J. Chem. Phys.* **121**, 7110 (2004).
- [36] S. Morita, R. Kaneko, and M. Imada, Quantum spin liquid in spin 1/2 J_1 - J_2 Heisenberg model on square lattice: Many-variable variational Monte Carlo study combined with

- quantum-number projections, *J. Phys. Soc. Jpn.* **84**, 024720 (2015).
- [37] Y. Nomura and M. Imada, Dirac-Type Nodal Spin Liquid Revealed by Refined Quantum Many-Body Solver Using Neural-Network Wave Function, Correlation Ratio, and Level Spectroscopy, *Phys. Rev. X* **11**, 031034 (2021).
- [38] D. Tahara and M. Imada, Variational Monte Carlo method combined with quantum-number projection and multi-variable optimization, *J. Phys. Soc. Jpn.* **77**, 114701 (2008).
- [39] G. Carleo and M. Troyer, Solving the quantum many-body problem with artificial neural networks, *Science* **355**, 602 (2017).
- [40] A. W. Sandvik, Finite-size scaling of the ground-state parameters of the two-dimensional Heisenberg model, *Phys. Rev. B* **56**, 11678 (1997).
- [41] J. Reuther and P. Wölfle, J_1 - J_2 frustrated two-dimensional Heisenberg model: Random phase approximation and functional renormalization group, *Phys. Rev. B* **81**, 144410 (2010).
- [42] P. Kopietz, L. Bartosch, and F. Schütz, Introduction to the functional renormalization group, *Lect. Notes Phys.* **798**, 380 (2010).
- [43] C. J. Halboth and W. Metzner, Renormalization-group analysis of the two-dimensional Hubbard model, *Phys. Rev. B* **61**, 7364 (2000).
- [44] L. Classen, A. V. Chubukov, C. Honerkamp, and M. M. Scherer, Competing orders at higher-order Van Hove points, *Phys. Rev. B* **102**, 125141 (2020).
- [45] D. Tarasevych and P. Kopietz, Dissipative spin dynamics in hot quantum paramagnets, *Phys. Rev. B* **104**, 024423 (2021).
- [46] A. A. Katanin, Fulfillment of Ward identities in the functional renormalization group approach, *Phys. Rev. B* **70**, 115109 (2004).
- [47] M. L. Baez and J. Reuther, Numerical treatment of spin systems with unrestricted spin length S : A functional renormalization group study, *Phys. Rev. B* **96**, 045144 (2017).
- [48] F. L. Buessen, D. Roscher, S. Diehl, and S. Trebst, Functional renormalization group approach to $SU(N)$ Heisenberg models: Real-space renormalization group at arbitrary N , *Phys. Rev. B* **97**, 064415 (2018).
- [49] Y. Iqbal, R. Thomale, F. Parisen Toldin, S. Rachel, and J. Reuther, Functional renormalization group for three-dimensional quantum magnetism, *Phys. Rev. B* **94**, 140408 (2016).
- [50] Y. Iqbal, H. O. Jeschke, J. Reuther, R. Valentí, I. I. Mazin, M. Greiter, and R. Thomale, Paramagnetism in the kagome compounds $(\text{Zn, Mg, Cd})\text{Cu}_3(\text{OH})_6\text{Cl}_2$, *Phys. Rev. B* **92**, 220404 (2015).
- [51] Y. Iqbal, P. Ghosh, R. Narayanan, B. Kumar, J. Reuther, and R. Thomale, Intertwined nematic orders in a frustrated ferromagnet, *Phys. Rev. B* **94**, 224403 (2016).
- [52] Y. Iqbal, T. Müller, K. Riedl, J. Reuther, S. Rachel, R. Valentí, M. J. P. Gingras, R. Thomale, and H. O. Jeschke, Signatures of a gearwheel quantum spin liquid in a spin- $\frac{1}{2}$ pyrochlore molybdate Heisenberg antiferromagnet, *Phys. Rev. Materials* **1**, 071201 (2017).
- [53] S. Chillal, Y. Iqbal, H. O. Jeschke, J. A. Rodriguez-Rivera, R. Bewley, P. Manuel, D. Khalyavin, P. Steffens, R. Thomale, A. T. M. N. Islam, J. Reuther, and B. Lake, Evidence for a three-dimensional quantum spin liquid in $\text{PbCuTe}_2\text{O}_6$, *Nat. Commun.* **11**, 2348 (2020).
- [54] Y. Iqbal, T. Müller, H. O. Jeschke, R. Thomale, and J. Reuther, Stability of the spiral spin liquid in MnSc_2S_4 , *Phys. Rev. B* **98**, 064427 (2018).
- [55] Y. Iqbal, T. Müller, P. Ghosh, M. J. P. Gingras, H. O. Jeschke, S. Rachel, J. Reuther, and R. Thomale, Quantum and Classical Phases of the Pyrochlore Heisenberg Model with Competing Interactions, *Phys. Rev. X* **9**, 011005 (2019).
- [56] M. Hering, J. Sonnenschein, Y. Iqbal, and J. Reuther, Characterization of quantum spin liquids and their spinon band structures via functional renormalization, *Phys. Rev. B* **99**, 100405 (2019).
- [57] P. Ghosh, T. Müller, F. P. Toldin, J. Richter, R. Narayanan, R. Thomale, J. Reuther, and Y. Iqbal, Quantum paramagnetism and helimagnetic orders in the Heisenberg model on the body centered cubic lattice, *Phys. Rev. B* **100**, 014420 (2019).
- [58] P. Ghosh, Y. Iqbal, T. Müller, R. T. Ponnaganti, R. Thomale, R. Narayanan, J. Reuther, M. J. P. Gingras, and H. O. Jeschke, Breathing chromium spinels: A showcase for a variety of pyrochlore Heisenberg Hamiltonians, *npj Quantum Mater.* **4**, 63 (2019).
- [59] K. Iida, H. K. Yoshida, A. Nakao, H. O. Jeschke, Y. Iqbal, K. Nakajima, S. Ohira-Kawamura, K. Munakata, Y. Inamura, N. Murai, M. Ishikado, R. Kumai, T. Okada, M. Oda, K. Kakurai, and M. Matsuda, $q = 0$ long-range magnetic order in centennialite $\text{CaCu}_3(\text{OD})_6\text{Cl}_2 \cdot 0.6\text{D}_2\text{O}$: A spin- $\frac{1}{2}$ perfect kagome antiferromagnet with J_1 - J_2 - J_d , *Phys. Rev. B* **101**, 220408 (2020).
- [60] D. Kiese, T. Mueller, Y. Iqbal, R. Thomale, and S. Trebst, Multiloop functional renormalization group approach to quantum spin systems, [arXiv:2011.01269](https://arxiv.org/abs/2011.01269).
- [61] I. Živković, V. Favre, C. Salazar Mejia, H. O. Jeschke, A. Magrez, B. Dabholkar, V. Nocolak, R. S. Freitas, M. Jeong, N. G. Hegde, L. Testa, P. Babkevich, Y. Su, P. Manuel, H. Luetkens, C. Baines, P. J. Baker, J. Wosnitza, O. Zaharko, Y. Iqbal *et al.*, Magnetic Field Induced Quantum Spin Liquid in the Two Coupled Trillium Lattices of $\text{K}_2\text{Ni}_2(\text{SO}_4)_3$, *Phys. Rev. Lett.* **127**, 157204 (2021).
- [62] M. Hering, V. Nocolak, F. Ferrari, Y. Iqbal, and J. Reuther, Dimerization tendencies of the pyrochlore Heisenberg antiferromagnet: A functional renormalization group perspective, [arXiv:2110.08160](https://arxiv.org/abs/2110.08160).
- [63] D. S. Rokhsar, Solitons in chiral-spin liquids, *Phys. Rev. Lett.* **65**, 1506 (1990).
- [64] The Rokhsar rules dictate that the optimal state at the mean-field level is given by a flux pattern where polygons with an odd number of sides (here, triangles) prefer to have a $\pi/2$ flux in order to minimize the fermion energy, while polygons with $4n$ sides (here, squares), where n is an integer, prefer to have π flux, and finally polygons with $4n + 2$ sides (the hexagons) prefer zero flux.
- [65] M. Hermele, T. Senthil, M. P. A. Fisher, P. A. Lee, N. Nagaosa, and X.-G. Wen, Stability of $U(1)$ spin liquids in two dimensions, *Phys. Rev. B* **70**, 214437 (2004).
- [66] X.-Y. Song, C. Wang, A. Vishwanath, and Y.-C. He, Unifying description of competing orders in two-dimensional quantum magnets, *Nat. Commun.* **10**, 4254 (2019).
- [67] The PW-VBC (L6-VBC) structure has six (eight) distinct symmetry inequivalent bonds/hopping amplitudes, and upon fixing one of them as the reference, we are left with five (seven) amplitudes which we optimize (see also SM [7]).

- [68] N. Astrakhantsev, T. Westerhout, A. Tiwari, K. Choo, A. Chen, M. H. Fischer, G. Carleo, and T. Neupert, Broken-Symmetry Ground States of the Heisenberg Model on the Pyrochlore Lattice, *Phys. Rev. X* **11**, 041021 (2021).
- [69] F. Verstraete and J. I. Cirac, Renormalization algorithms for quantum-many body systems in two and higher dimensions, [arXiv:cond-mat/0407066](https://arxiv.org/abs/cond-mat/0407066).
- [70] J. Jordan, R. Orús, G. Vidal, F. Verstraete, and J. I. Cirac, Classical Simulation of Infinite-Size Quantum Lattice Systems in Two Spatial Dimensions, *Phys. Rev. Lett.* **101**, 250602 (2008).
- [71] H. J. Liao, Z. Y. Xie, J. Chen, Z. Y. Liu, H. D. Xie, R. Z. Huang, B. Normand, and T. Xiang, Gapless Spin-Liquid Ground State in the $S = 1/2$ Kagome Antiferromagnet, *Phys. Rev. Lett.* **118**, 137202 (2017).
- [72] T. Picot and D. Poilblanc, Nematic and supernematic phases in kagome quantum antiferromagnets under the influence of a magnetic field, *Phys. Rev. B* **91**, 064415 (2015).
- [73] A. Kshetrimayum, C. Balz, B. Lake, and J. Eisert, Tensor network investigation of the double layer Kagome compound $\text{Ca}_{10}\text{Cr}_7\text{O}_{28}$, *Ann. Phys.* **421**, 168292 (2020).
- [74] C. Boos, S. P. G. Crone, I. A. Niesen, P. Corboz, K. P. Schmidt, and F. Mila, Competition between intermediate plaquette phases in $\text{SrCu}_2(\text{BO}_3)_2$ under pressure, *Phys. Rev. B* **100**, 140413 (2019).
- [75] H. C. Jiang, Z. Y. Weng, and T. Xiang, Accurate Determination of Tensor Network State of Quantum Lattice Models in Two Dimensions, *Phys. Rev. Lett.* **101**, 090603 (2008).
- [76] T. Picot, M. Ziegler, R. Orús, and D. Poilblanc, Spin- S kagome quantum antiferromagnets in a field with tensor networks, *Phys. Rev. B* **93**, 060407 (2016).
- [77] A. Kshetrimayum, T. Picot, R. Orús, and D. Poilblanc, Spin- $\frac{1}{2}$ kagome XXZ model in a field: Competition between lattice nematic and solid orders, *Phys. Rev. B* **94**, 235146 (2016).
- [78] T. Nishino and K. Okunishi, Corner transfer matrix renormalization group method, *J. Phys. Soc. Jpn.* **65**, 891 (1996).
- [79] T. Nishino and K. Okunishi, Corner transfer matrix algorithm for classical renormalization group, *J. Phys. Soc. Jpn.* **66**, 3040 (1997).
- [80] R. Orús and G. Vidal, Simulation of two-dimensional quantum systems on an infinite lattice revisited: Corner transfer matrix for tensor contraction, *Phys. Rev. B* **80**, 094403 (2009).
- [81] R. Orús, Exploring corner transfer matrices and corner tensors for the classical simulation of quantum lattice systems, *Phys. Rev. B* **85**, 205117 (2012).
- [82] A. M. Tsvelik, New Fermionic Description of Quantum Spin Liquid State, *Phys. Rev. Lett.* **69**, 2142 (1992).
- [83] N. Niggemann, B. Sbierski, and J. Reuther, Frustrated quantum spins at finite temperature: Pseudo-Majorana functional renormalization group approach, *Phys. Rev. B* **103**, 104431 (2021).
- [84] A. Lohmann, H.-J. Schmidt, and J. Richter, Tenth-order high-temperature expansion for the susceptibility and the specific heat of spin- s Heisenberg models with arbitrary exchange patterns: Application to pyrochlore and kagome magnets, *Phys. Rev. B* **89**, 014415 (2014).
- [85] N. Niggemann, J. Reuther, and B. Sbierski, Quantitative functional renormalization for three-dimensional quantum Heisenberg models, [arXiv:2112.08104](https://arxiv.org/abs/2112.08104).
- [86] <http://ckp.nrcki.ru>.
- [87] L. Bennett, B. Melchers, and B. Proppe, Curta: A general-purpose high-performance computer at ZEDAT, Freie Universität Berlin (2020).
- [88] www.gauss-centre.eu.
- [89] www.lrz.de.